

Electronic Supporting Information (ESI)

## Complex-shaped hydrogels by diffusion controlled gelation of nanocellulose crystallites

C. A. Maestri,<sup>a,b</sup> P. Bettotti<sup>a</sup> and M. Scarpa<sup>a\*</sup>

<sup>a</sup>Nanoscience Laboratory, Department of Physics, University of Trento, Via Sommarive 14, 38123 Povo (TN), Italy \*Email - marina.scarpa@unitn.it

<sup>b</sup>Centre for integrative Biology, University of Trento, Via Sommarive 9, 38123 Povo (TN), Italy

### A) NC-Ca<sup>2+</sup> ionotropic gel structures..

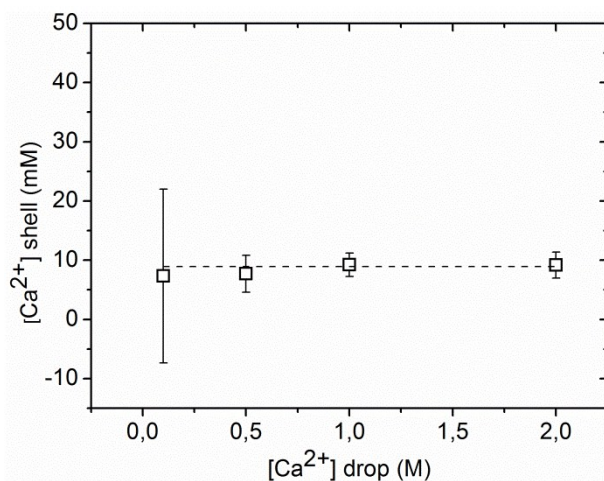


**Fig. S1:** Concentration of Ca<sup>2+</sup> ions in the shell of NC-Ca<sup>2+</sup> capsules obtained by inverse ionotropic gelation as a function of Ca<sup>2+</sup> concentration in the starting CaCl<sub>2</sub> solution drop.

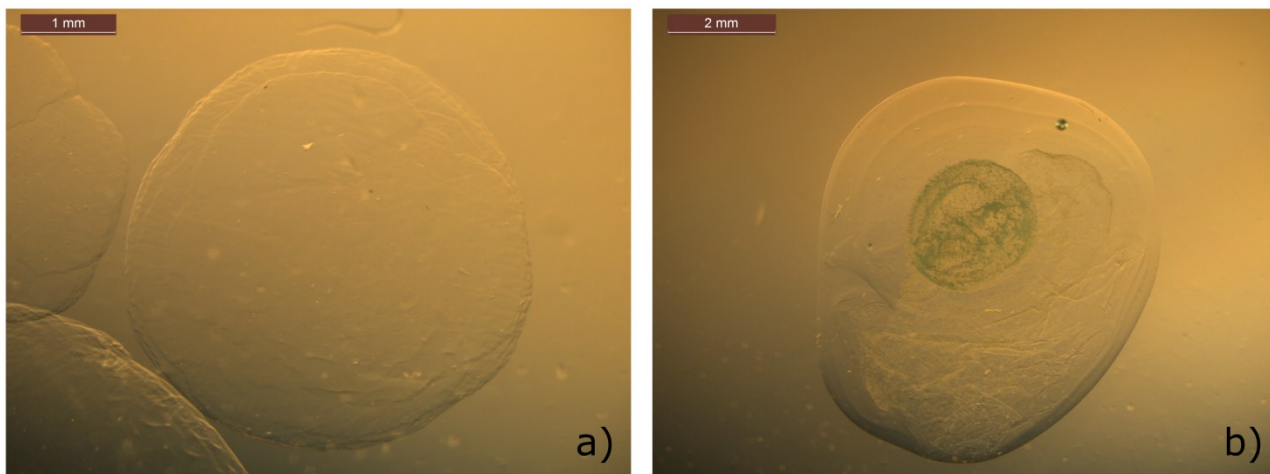


**Fig. S2:** Optical images of a NC-Ca<sup>2+</sup> bead (a) and of a NC-Ca<sup>2+</sup> core-shell capsule (b) obtained by external and inverse ionotropic gelation, respectively. Images were acquired on gel structures suspended in pure water using a Leica MZ 16 FA stereomicroscope.

### **B) FTIR characterization of dried NC-Ca<sup>2+</sup> beads.**

The COO<sup>-</sup> symmetric and asymmetric stretching vibration bands are fingerprints of TEMPO-oxidized nanocellulose crystallites and their position depends on the complexation by the counter ions. Here we used the position of the symmetric and asymmetric carboxylate peaks centered at 1410 cm<sup>-1</sup> and 1608 cm<sup>-1</sup> in NC films, where the counter ion of the carboxylate groups is Na<sup>+</sup>, and at 1420 cm<sup>-1</sup> and 1600 cm<sup>-1</sup> in NC-Ca<sup>2+</sup> hydrogels, where the counter ion is Ca<sup>2+</sup>, respectively, to monitor the presence of Ca<sup>2+</sup> in the hydrogel, as suggested by Papageorgiou et al. for alginate complexes<sup>1</sup>. Figure S3 (a) compares the spectra of a NC film (gray dotted line) and of a dried NC-Ca<sup>2+</sup> gel bead (black continuous line), while Figure S3 (b) shows the wavenumber shift of asymmetric band toward smaller wavenumbers and of symmetric band toward higher wavenumbers upon Ca<sup>2+</sup> complexation. The analysis of the FTIR spectra was performed after: a) deconvolution of the partially overlapping peaks and b) normalization of the intensities with respect to the 1372 cm<sup>-1</sup> peak, which is related to the in-plane alkane -C-H bending vibration in NC and can be assumed to be constant for all the samples and not altered by the ionotropic gelation.<sup>2</sup> The bands at around 1610 cm<sup>-1</sup> were analyzed performing a double gaussian fit procedure to separate the contribution of the asymmetric carboxylate stretching vibration from that of water (at 1640 cm<sup>-1</sup>). The bands at around 1420 cm<sup>-1</sup> were analyzed in NC films performing a double gaussian fit procedure to separate the contribution of the symmetric carboxylate

stretching vibration from that of alkane -C-H vibrations (at  $1425\text{ cm}^{-1}$ ). The obtained alkane peaks were subtracted from NC-Ca<sup>2+</sup> spectra to isolate the symmetric carboxylate stretching vibration peak. The assignments of the main vibrational peaks typical of TEMPO-oxidized cellulose samples are reported in Table S1, while the specific data for the COO<sup>-</sup> bands are summarized in Table S2 for both NC films and NC-Ca<sup>2+</sup> hydrogels .

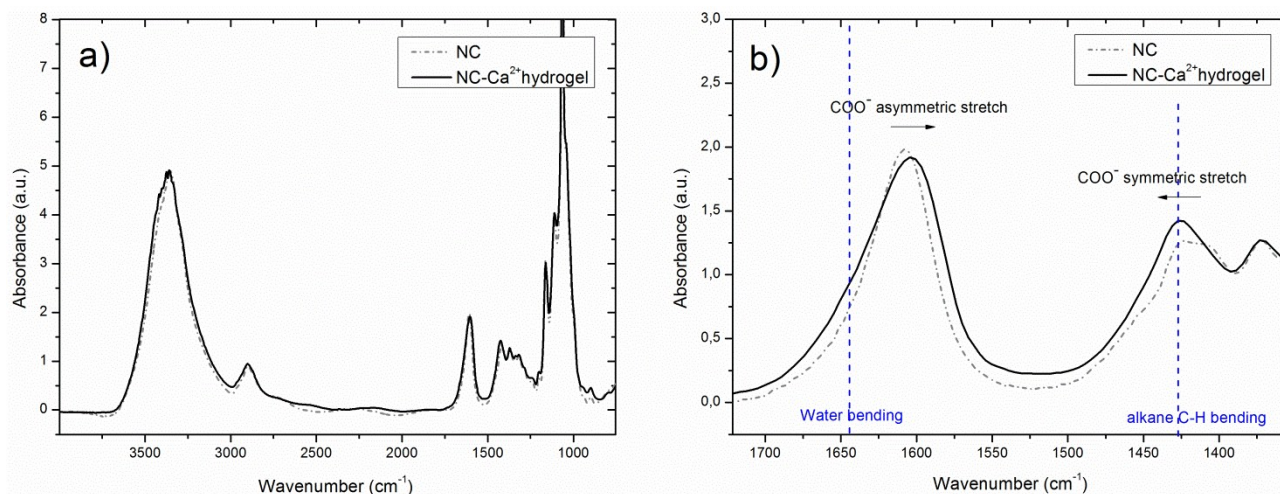


**Fig. S3:** (a) FTIR spectra of a NC film (gray dotted line) prepared by casting a solution of as-prepared NC at pH 7.0 and of a dried NC-Ca<sup>2+</sup> gel bead fragment obtained by external ionotropic gelation (black continuous line) (b) Zoom on the  $1300\text{-}1750\text{ cm}^{-1}$  range where the carboxylate stretching bands are located, with assignment of the main vibrational bands present in the region<sup>2</sup>. The dashed vertical lines indicate the wavenumbers where water bending vibration mode and alkane C-H bending mode are located. The spectra were acquired in transmission mode with  $1\text{ cm}^{-1}$  spectral resolution on a micro-FTIR Nicolet iN10 instrument equipped with a liquid nitrogen cooled detector.

Vibrational band assignment	peak position
O-H stretching	3300-3400 cm <sup>-1</sup>
C-H stretching (CH <sub>2</sub> )	2900 cm <sup>-1</sup>
O-H bending of adsorbed water	1640 cm <sup>-1</sup>
COO <sup>-</sup> asymmetric stretching	1600-1610 cm <sup>-1</sup>
HCH and OCH in-plane bending	1425 cm <sup>-1</sup>
COO <sup>-</sup> symmetric stretching	1410-1420 cm <sup>-1</sup>
CH in-plane bending	1370 cm <sup>-1</sup>
CH <sub>2</sub> rocking at C <sub>6</sub>	1317 cm <sup>-1</sup>
C-O-C stretching	1161 cm <sup>-1</sup>
C-C stretching	1112 cm <sup>-1</sup>

**Table S1:** Assignations of the main vibrational bands observed in TEMPO-oxidized nanocellulose samples and reported in Fig. S3 (a).<sup>2</sup>

	$\nu(\text{COO}^-_{\text{asymm}})$ [cm <sup>-1</sup> ]	$\nu(\text{COO}^-_{\text{symm}})$ [cm <sup>-1</sup> ]	$I(\text{COO}^-_{\text{asymm}})$ [a.u.]	$I(\text{COO}^-_{\text{symm}})$ [a.u.]
<b>NC-film</b>	1608.3 ± 0.3	1410 ± 3	2.0 ± 0.2	1.2 ± 0.3
<b>NC-Ca<sup>2+</sup></b>	1601 ± 1	1419 ± 2	1.8 ± 0.1	1.05 ± 0.05

**Table S2:** Results of spectral analysis performed on NC films and NC-Ca<sup>2+</sup> hydrogels. Peak centers and peak absorbance intensity for both COO<sup>-</sup> asymmetric and symmetric bands are reported. Values and errors refer to mean values and standard deviation over at least 10 measurements.

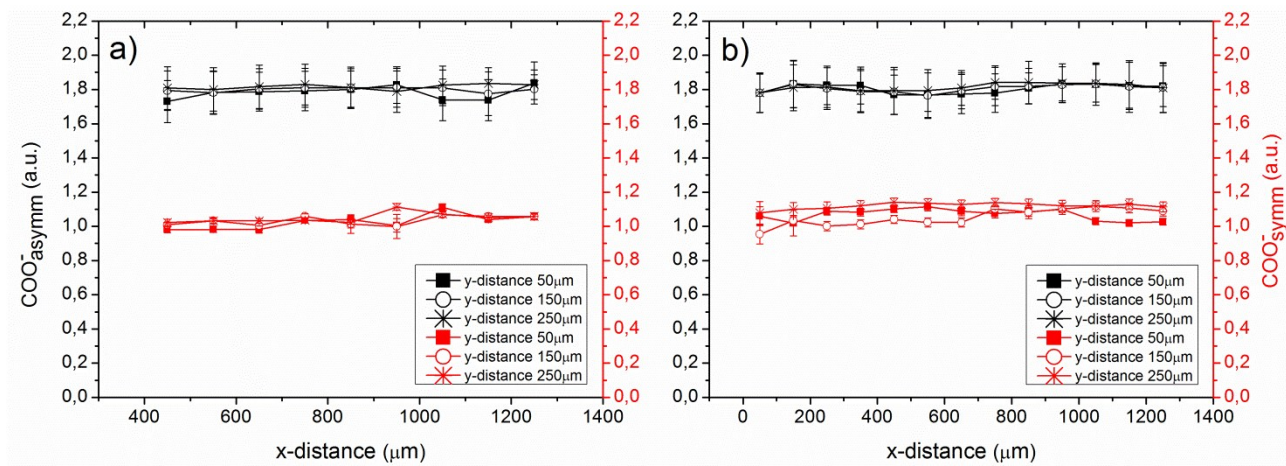


**Fig. S4:** Intensity of  $\text{COO}^-$  asymmetric (black traces) and  $\text{COO}^-$  symmetric (red traces) absorption peaks. The x and y distances reported on the x-axis and in the legend refer, respectively, to the xy centre position of the  $100 \times 100 \mu\text{m}$  area corresponding to each map point spectrum. Left panel and right panel refer to an area near the surface and at the centre of the dried sample, respectively.

### C) Determination of $\text{Ca}^{2+}$ by murexide.

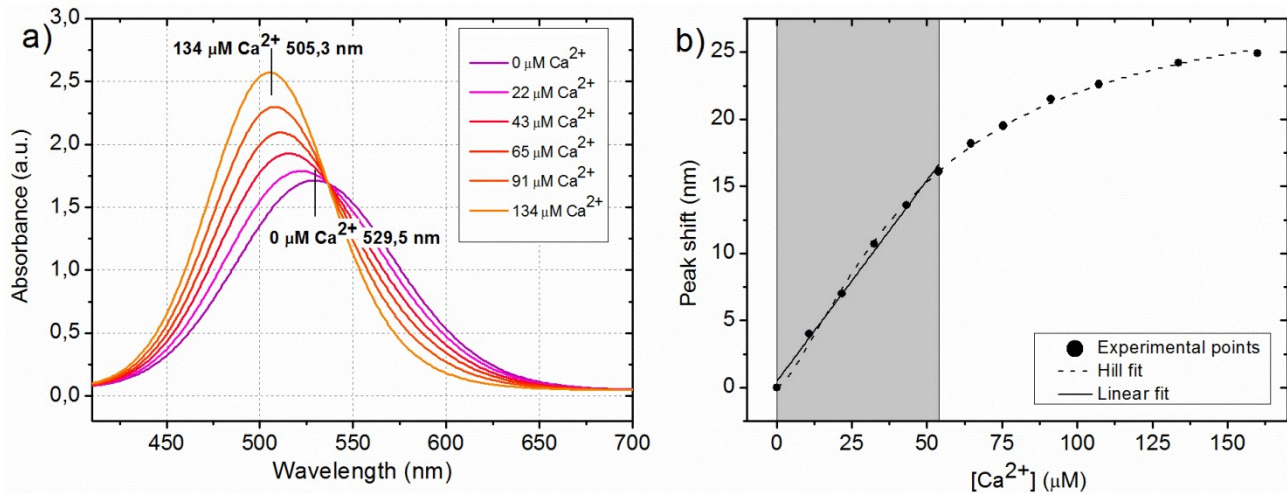


**Fig. S5:** (a) Murexide absorption peak in the presence of increasing  $\text{Ca}^{2+}$  concentrations. The absorption peak of 0.2 mM murexide at pH 11.3 is centered at around 529.5 nm in absence of  $\text{Ca}^{2+}$  and progressively moves to shorter wavelengths by adding  $\text{Ca}^{2+}$ . (b) Peak shift versus  $\text{Ca}^{2+}$  concentration. The experimental points were fitted to a Hill curve  $y = V_{\max} x^n / (k^n + x^n)$  and the resulting  $V_{\max}$ ,  $k$  and  $n$  parameters were used to determine  $\text{Ca}^{2+}$  concentration released into aqueous solutions by NC- $\text{Ca}^{2+}$  hydrogels. The gray area highlights the concentration range involved in the  $\text{Ca}^{2+}$  release of the measurements performed in the present work. The spectra were acquired by a Varian-Cary 5000 UV-VIS-NIR spectrophotometer operated in the range 200-900 nm with a 1 nm resolution.

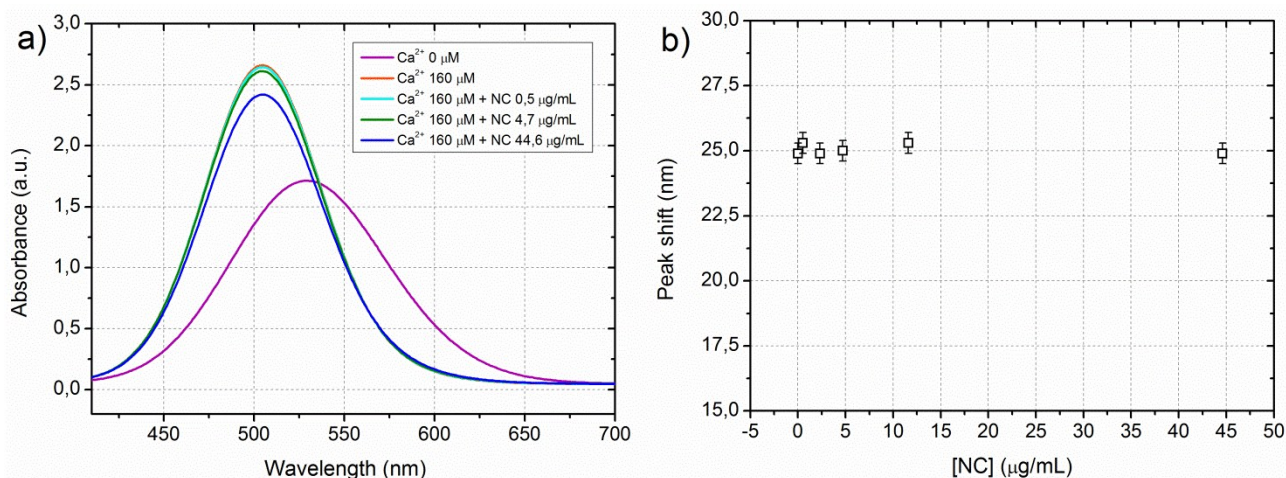


**Fig. S6:** Effect of NC on murexide- $\text{Ca}^{2+}$  peak position. Various concentrations of NC (from 0.5 to 45  $\mu\text{g mL}^{-1}$ ) were added to a solution containing murexide (0.2 mM) and  $\text{Ca}^{2+}$  (160  $\mu\text{M}$ ) to check that NC crystallites do not interfere with  $\text{Ca}^{2+}$  determination. a) Absorbance spectra of murexide- $\text{Ca}^{2+}$  solutions after addition of different amounts of NC crystallites (from 0.5  $\mu\text{M}$  to 45  $\mu\text{M}$ ). As a comparison, the spectrum of murexide in the absence of  $\text{Ca}^{2+}$  is reported (purple trace). b) Shift of absorbance peak of murexide- $\text{Ca}^{2+}$  solutions (murexide 0.2 mM,  $\text{Ca}^{2+}$  160  $\mu\text{M}$ ) after addition of different amounts of NC. Peak shift was calculated with respect to the maximum absorbance of murexide in the absence of  $\text{Ca}^{2+}$  (peak at 529.5 nm).

#### D) NC- $\text{Ca}^{2+}$ hydrogels stability in water

NC- $\text{Ca}^{2+}$  hydrogels are stable in water for months. The only effect of long-times water incubation is a slightly reduced compactness, as qualitatively visible in Fig. S6, and increased dimension, as shown in Fig. S7, where the factor  $\Delta V$  is the volumetric swelling ratio, defined as

$$\Delta V = \frac{V_{\text{swollen in water}} - V_{\text{hydrogel}}}{V_{\text{hydrogel}}} \times 100$$



**Fig. S7:** Images of NC-Ca<sup>2+</sup> beads obtained by external ionotropic gelation and incubated in distilled water for 9 months and of NC-Ca<sup>2+</sup> beads immediately after the external ionotropic gelation process.

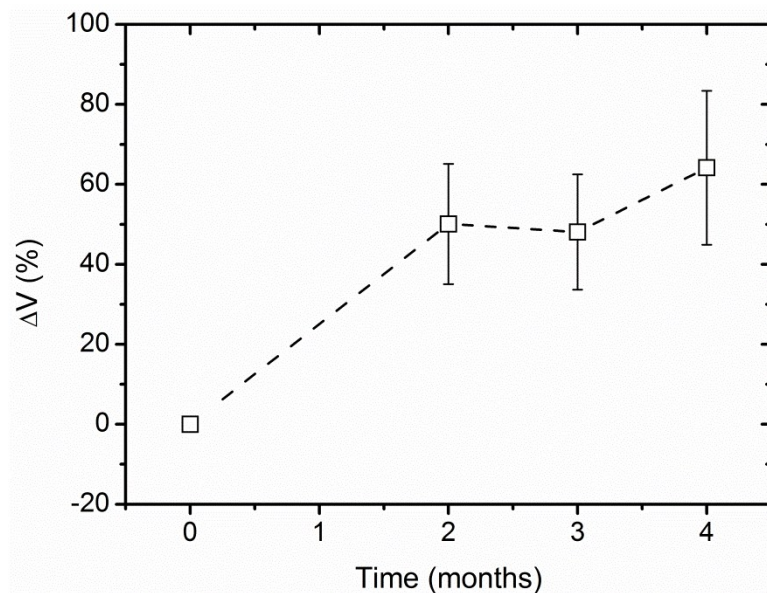


**Fig. S8:** Volumetric swelling ratio for NC-Ca<sup>2+</sup> hydrogel beads obtained by external ionotropic gelation (NC concentration  $8 \pm 1$  mg mL<sup>-1</sup> and CaCl<sub>2</sub> concentration 1 M) as a function incubation time in water.

### E) $\text{Ca}^{2+}$ diffusion and external ionotropic gelation kinetic

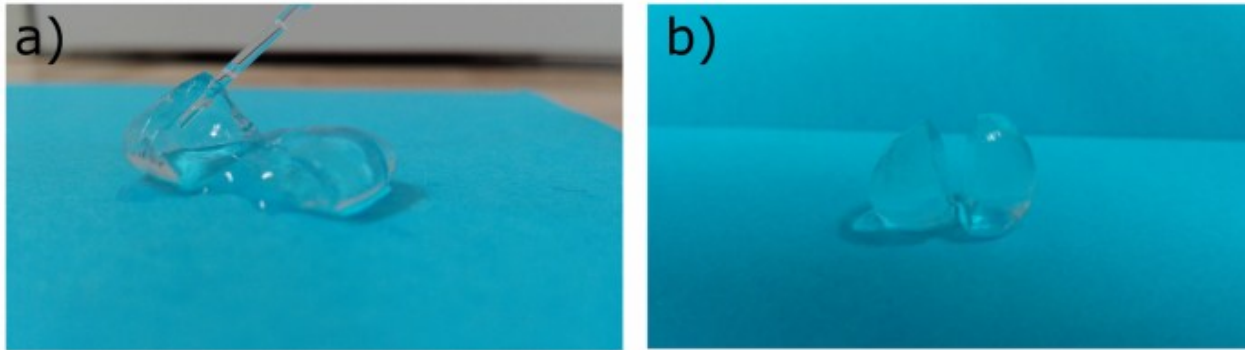


**Fig. S9:** Bead of NC- $\text{Ca}^{2+}$  hydrogel obtained via external ionotropic gelation after (a) 30sec and (b) 10min in 1M  $\text{CaCl}_2$  solution.

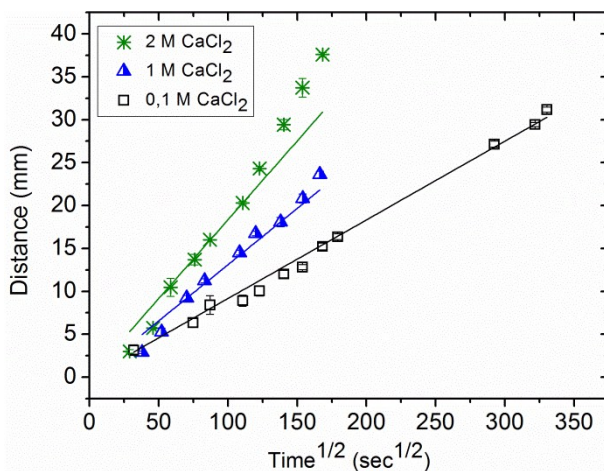


**Fig. S10.** Sol-gel front distance from dialysis membrane as a function of square root of time for constant concentration of NC ( $8 \text{ mg mL}^{-1}$ ) and murexide ( $20 \text{ }\mu\text{M}$ ) and different  $\text{CaCl}_2$  concentrations. The points and errors are the mean value and standard deviation, respectively. The lines are linear fits (with intercept fixed to 0) performed on each set of data. The slopes resulting from the linear fits are  $(92 \pm 1) \text{ }\mu\text{m sec}^{-1/2}$ ,  $(139 \pm 6) \text{ }\mu\text{m sec}^{-1/2}$  and  $(184 \pm 6) \text{ }\mu\text{m sec}^{-1/2}$  respectively for 0.1 M, 1 M and 2 M  $\text{CaCl}_2$  solutions.

## F) $\text{Ca}^{2+}$ diffusion and inverse ionotropic gelation kinetic

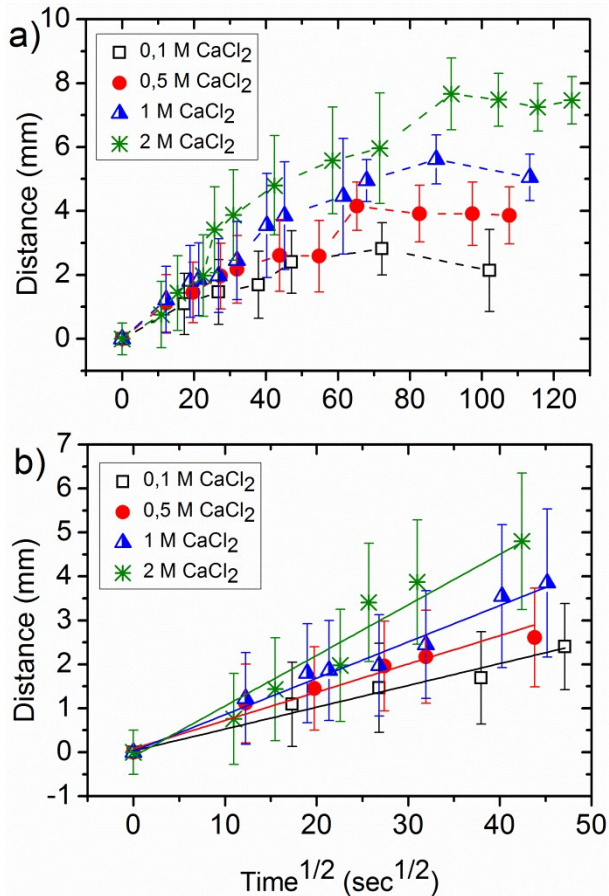


**Fig. S11.** Gel growth measurements for inverse ionotropic gelation. (a) Sol-gel front distance from the inner liquid core as a function of square root of time for constant NC-Murexide solution concentrations (NC 8 mg mL<sup>-1</sup>, murexide 20 μM) and different CaCl<sub>2</sub> concentrations. The points and errors are the mean value and standard deviation, respectively. (b) Zoom on the short-times region characterized by a linear trend. The lines are linear fits performed on each set of data. The slopes resulting from the linear fits are  $(50 \pm 4) \mu\text{m sec}^{-1/2}$ ,  $(64 \pm 5) \mu\text{m sec}^{-1/2}$ ,  $(83 \pm 4) \mu\text{m sec}^{-1/2}$  and  $(115 \pm 10) \mu\text{m sec}^{-1/2}$  respectively for 0.1 M, 0.5 M, 1 M and 2 M CaCl<sub>2</sub> solutions.

## G) Reaction-diffusion models

### Analytical model for the reaction front as a function of time.

Reaction-diffusion systems showing a reaction front which evolves in time are characteristic of many physical, chemical and biological processes.<sup>3,4</sup> In 1988 Racz and Galfi<sup>5</sup> proposed an analytical model (known as "mean field model") for the reaction front in the case of a chemical reaction  $A_{(diffusing)} + B_{(diffusing)} \rightarrow C_{(inert)}$ , where the reagents A and B (initially separated in space) react to produce the inert species C and the reaction kinetics is of second order. Aim of the model is to obtain a scaling description for the center and width of the reaction front and for the production rate of C starting from a couple of reaction-diffusion equations. Later on, Leger et al.<sup>6</sup> experimentally studied the case  $A_{(diffusing)} + B_{(static)} \rightarrow C_{(inert)}$  and demonstrated that the results obtained by Racz and Galfi for the movement of the reaction front as a function of time is independent of the reaction orders or the number of diffusing reactants (one or two) as long as the two species are initially separated and there is no relative advection of them. In particular, the model can be used to describe the ionotropic gelation process of NC in presence of  $Ca^{2+}$  ions, where  $A_{(diffusing)} = Ca^{2+}$  ions,  $B_{(static)} = NC$  and  $C_{(inert)} = NC-Ca^{2+}$  hydrogel. Here we recall how, from the model, the characteristic distance versus time<sup>1/2</sup> relationship observed experimentally can be analytically obtained and how the apparent diffusion coefficient is introduced. The mathematical description of the considered reaction-diffusion process is given by the following set of reaction-diffusion equations:

$$\frac{\partial a}{\partial t} = D_a \frac{\partial^2 a}{\partial x^2} - kab \quad (1)$$

$$\frac{\partial b}{\partial t} = D_b \frac{\partial^2 b}{\partial x^2} - kab \quad (2)$$

where  $a, b$  are the concentrations of the reactants A and B,  $D_a$  and  $D_b$  the diffusion constants and  $k$  the reaction rate constant. The model is developed in 1D, where  $x$  is the spatial coordinate, and considering, as an initial condition, A, B separated and with constant densities:  $a = a_0$  and  $b = 0$ , for  $x <$

0 and  $a = 0$  and  $b = b_0$  for  $x > 0$ . For simplicity we consider  $D_a = D_b = D$  (same conclusions can be obtained in the case  $D_a \neq D_b$ ). We introduce the units  $l = \sqrt{D/(ka_0)}$ ,  $\tau = 1/(ka_0)$  and  $a_0$  to measure lengths, time and concentration, so that the only control parameter remains  $q = b_0/a_0$ . Subtracting Eq. (2) from Eq. (1) we obtain a diffusion equation for  $u = a - b$ :

$$\frac{\partial u}{\partial t} = D \frac{\partial^2 u}{\partial x^2} \quad (3)$$

that can be solved with the initial conditions  $u = 1$  ( $x < 0$ ) and  $u = -q$  ( $x > 0$ ) obtaining:

$$u(x,t) = \frac{1-q}{2} + \frac{1+q}{2} \operatorname{erf}\left(\frac{x}{2\sqrt{t}}\right) \quad (4)$$

Where  $\operatorname{erf}(x) = \frac{1}{\sqrt{\pi}} \int_{-x}^x e^{-t^2} dt$  is the error function. We introduce now a reference point  $x_f$ , assumed as the center of the reaction zone, where  $a = b$  and the production rate of C is expected to be the largest. This point can be determined from Eq. (4) by requiring  $a(x_f, t) = b(x_f, t)$ , that is  $u(x_f, t) = 0$ . The time dependence of  $x_f$  is:

$$x_f = \sqrt{2D_f t} \quad (5)$$

where  $D_f$  is the "diffusion constant" of the front (or apparent diffusion coefficient) given by the equation:

$$\operatorname{erf}\left(\sqrt{D_f/2}\right) = (1-q)/(1+q) \quad (6)$$

### Steady state model for gel growth kinetics.

In order to explain the experimentally observed kinetics and obtain the real diffusion coefficient of  $\text{Ca}^{2+}$  ions through the NC- $\text{Ca}^{2+}$  hydrogel, a model is required that relates front propagation kinetics and  $\text{Ca}^{2+}$  diffusion. Different models exist in literature depending on the particular experimental conditions and geometry.<sup>7-10</sup> Here we report a model based on the theory developed by Braschler et

al.,<sup>9</sup> who studied the  $\text{Ca}^{2+}$ -induced gelation of alginate systems both analytically and experimentally by following the sol-gel front propagation using fluorescence intensity signals. The presented reaction-diffusion model is essentially based on two mechanisms: the chemical reaction between nanocellulose crystallites and  $\text{Ca}^{2+}$  ions and the diffusion of the reactants (in particular the flux  $J_C$  of  $\text{Ca}^{2+}$  ions, as we assume the diffusion of nanocellulose crystallites negligible). In Fig. S12 we show a schematic view of the 1D reaction-diffusion system with the main quantities considered in the model.

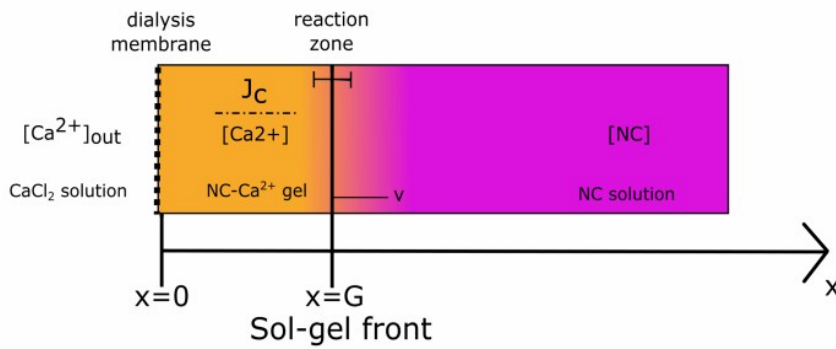


**Fig. S12:** Schematic view of the reaction-diffusion system involved in the proposed model. To reach the reaction front and promote the gelation of NC solution by chemically reacting with it,  $\text{Ca}^{2+}$  ions have to diffuse through the already formed gel. The concentration of free NC in the gel can be assumed to be very low, so that negligible reaction takes place in it. The transport of free  $\text{Ca}^{2+}$  ions through the gel is studied as a linear diffusion process. The advancement of the reaction front is determined by the flux of  $\text{Ca}^{2+}$  ions  $J_C$  and the stoichiometry of the NC- $\text{Ca}^{2+}$  reaction.

In the hypothesis that the  $\text{Ca}^{2+}$  ions flux converts a known amount of NC crystallites and that the flux of nanocellulose  $J_{NC} = v [NC]$  consumed by the reaction is equal to the flux of  $\text{Ca}^{2+}$  ions  $J_C$  reaching the reaction zone, we have:

$$J_c = R J_{NC} = R v [NC] \quad (7)$$

where  $R$  is a factor taking into account the NC- $\text{Ca}^{2+}$  reaction stoichiometry,  $v$  is the advancing speed of the reaction front and  $[NC]$  the bulk nanocellulose concentration. As there is little free NC in the gel region, the reaction rate is very low and the transport of  $\text{Ca}^{2+}$  ions through the gel is regulated by the linear diffusion equation:

$$D_c \frac{\partial^2 [Ca^{2+}]}{\partial x^2} - \frac{\partial [Ca^{2+}]}{\partial t} \approx 0 \quad (8)$$

where  $D_c$  is the  $Ca^{2+}$  diffusion coefficient in the gel,  $[Ca^{2+}]$  the calcium concentration and  $x$  the spatial coordinate of the gel growth in 1D (as illustrated in Fig. S12). To solve Eq. (8), two boundary conditions are required. The first one is obtained from the fact that the concentration of free  $Ca^{2+}$  ions is low in the reaction zone ( $x = G$ ), that is:

$$[Ca^{2+}]_{x=G} \approx 0 \quad (9)$$

The problem of a mobile boundary which advances with a speed given by the diffusive transport of a reactant whose concentration is zero at the reaction front is known as Stefan problem.<sup>11</sup> The second boundary condition arises from Fick's law of diffusion at the dialysis membrane ( $x = 0$ ) and results to be:

$$\left( \frac{\partial [Ca^{2+}]}{\partial x} \right)_{x=0} = \frac{[Ca^{2+}]_{(x=0)} - [Ca^{2+}]_{out}}{L} \quad (10)$$

where  $L$  is the thickness of the dialysis membrane and  $[Ca^{2+}]_{out}$  the bulk concentration of  $Ca^{2+}$  ions outside the dialysis membrane ( $x < 0$ ). An approximated analytical solution of eq 8 with boundary conditions given by Eq. (9) and Eq. (10) can be obtained in the hypothesis that  $\frac{\partial [Ca^{2+}]}{\partial t} = 0$  (steady-state concentration gradient for the  $Ca^{2+}$  ions). This assumption is known as Kim's model and is typically used in alginate gel growth studies.<sup>12</sup> In this approximation, the concentration of free  $Ca^{2+}$  ions in the gel is:

$$[Ca^{2+}] = [Ca^{2+}]_{out} \frac{x}{G + L} \quad (11)$$

meaning a constant flux  $J_c$  through the gel:

$$J_c = D_c \frac{[Ca^{2+}]_{out}}{G + L} \quad (12)$$

Combining Eq. (7) with Eq. (12) and considering that  $v = \frac{\partial G}{\partial t}$  we obtain:

$$\frac{\partial G}{\partial t} = \frac{D_c \theta}{G + L} \quad (13)$$

where we have introduced  $\theta = \frac{[Ca^{2+}]_{out}}{R [NC]}$  as a shorthand notation for the ratio between the bulk  $Ca^{2+}$  concentration  $[Ca^{2+}]_{out}$  and the nanocellulose crystallites concentration  $[NC]$  multiplied by the factor  $R$ , which accounts for both the carboxylic content of TEMPO oxidized NC crystallites and the stoichiometry of the NC- $Ca^{2+}$  reaction. The solution of Eq. (12) gives an expression for the temporal progression of the reaction front in the x-direction:

$$G(t) = \sqrt{2D_c \theta * t + L^2} - L \approx \sqrt{2D_c \theta * t} \quad (14)$$

Eq. (14) confirms the characteristic dependence of front propagation  $G(t)$  on  $t^{1/2}$ . Moreover it allows to estimate  $Ca^{2+}$  ions diffusion coefficient in the gel starting from the slope of the curve  $K = \frac{G(t)}{\sqrt{t}}$  or

from the apparent diffusion coefficient  $D_f = \frac{G(t)^2}{2t}$  :

$$D_c = \frac{K^2}{2\theta} = \frac{D_f}{\theta} \quad (15)$$

The only factor which is still unknown and prevent us from estimating  $D_c$  is the  $\theta$  factor, because of  $R$ . While  $R$  is quite well settled for some reaction-diffusion systems (like the case of alginate- $Ca^{2+}$  gels studied by Braschler et al.) it is still unknown for NC- $Ca^{2+}$  hydrogels because of the lack of information regarding the precise stoichiometry of  $Ca^{2+}$ -nanocellulose interaction. A different formulation of the  $\theta$  factor, which can be evaluated in our NC- $Ca^{2+}$  systems too, is suggested by M. Nobe et al.<sup>10</sup> who

studied the  $\text{Ca}^{2+}$ -induced gelification of Curdlan polysaccharide following the front line progress and by Furusawa et al.<sup>13</sup> who investigated the gelification of DNA upon cobalt ions diffusion. According to their models, the  $\theta$  factor relating  $\text{Ca}^{2+}$  diffusion and apparent diffusion coefficient can be estimated as:

$$\theta \approx \frac{\rho_s}{\rho_G} \quad (16)$$

where  $\rho_s = [\text{Ca}^{2+}]_{out}$  and  $\rho_G$  is the critical salt concentration for forming the hydrogel (dependent on the salt-polysaccharide/DNA interaction and polysaccharide/DNA concentration) which can be obtained experimentally.

#### H) Morphological characterization of nanocellulose crystallites.

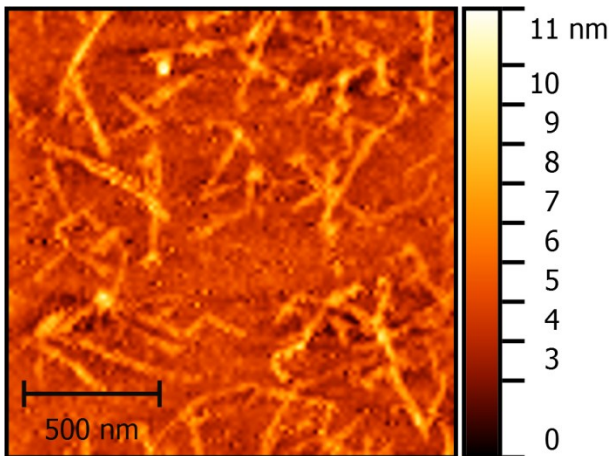


**Fig. S13.** AFM image of NC obtained by TEMPO-mediated oxidation and sonication. A drop of a diluted NC suspension was deposited over a flat silicon support and the solvent was left to dry completely under a gentle nitrogen flow. The image was acquired by an AFM NT-MDT P47H scanning probe microscope operated in semi contact mode.

#### References:

- 1 S. K. Papageorgiou, E. P. Kouvelos, E. P. Favvas, A. A. Sapalidis, G. E. Romanos and F. K. Katsaros, *Carbohydr. Res.*, 2010, **345**, 469–473.
- 2 B. Li, W. Xu, D. Kronlund, A. Määttä, J. Liu, J.-H. Smått, J. Peltonen, S. Willför, X. Mu and C. Xu, *Carbohydr. Polym.*, 2015, **133**, 605–612.
- 3 S. Kondo and T. Miura, *Science*, 2010, **329**, 1616–1620.
- 4 M. Cencini, C. Lopez and D. Vergni, in *The Kolmogorov Legacy in Physics*, Springer, 2003, pp. 187–210.
- 5 L. Gálfi and Z. Rácz, *Phys. Rev. A*, 1988, **38**, 3151.
- 6 C. Léger, F. Argoul and M. Z. Bazant, *J. Phys. Chem. B*, 1999, **103**, 5841–5851.
- 7 K. Potter, B. J. Balcom, A. Carpenter and L. Hall, *Carbohydr. Res.* 1994, **257**, 117–126.
- 8 S. H. Bjørnøy, S. Mandaric, D. C. Bassett, A. K. O. Åslund, S. Ucar, J.-P. Andreassen, B. L. Strand and P. Sikorski, *Acta Biomater.*, 2016, **44**, 243–253.
- 9 T. Braschler, A. Valero, L. Colella, K. Pataky, J. Brugger and P. Renaud, *Anal. Chem.*, 2011, **83**, 2234–2242.
- 10 M. Nobe, T. Dobashi and T. Yamamoto, *Langmuir*, 2005, **21**, 8155–8160.
- 11 D. Hilhorst, R. Van der Hout and L. A. Peletier, *Math. Anal. Appl.*, 1996, **199**, 349–373.
- 12 H.-S. Kim, *Korean J. Chem. Eng.*, 1990, **7**, 1–6.
- 13 K. Furusawa, Y. Minamisawa, T. Dobashi and T. Yamamoto, *J. Phys. Chem. B*, 2007, **111**, 14423–14430.